Available online at www.sciencedirect.com
SCIENCE DIRECT®
PERGAMON
International Journal of Heat and Mass Transfer 46 (2003) 5017–5030
International Journal of HEAT and MASS TRANSFER
www.elsevier.com/locate/ijhmt

Non-thermal equilibrium melting of granular packed bed in horizontal forced convection. Part I: experiment

Y.L. Hao, Y.-X. Tao *

Department of Mechanical and Materials Engineering, Florida International University, Miami, FL 33199, USA

Received 6 March 2003; received in revised form 2 July 2003

Abstract

A series of experiments are conducted to investigate the non-thermal equilibrium characteristics of melting of a packed bed under horizontal forced and mixed convections. This configuration imposes a complex treatment in phase change heat transfer that involves not only the coupled heat, mass and momentum exchanges but also the local geometric change of the packed bed (packing effect). Using visualization observations and measurements, we determine experimentally the volumes and packing patterns of the melting granular packed beds and the time variation of average melting rate per unit bed volume and average heat transfer coefficient for $Re = 71$–2291, $Gr/Re^2 = 1.48 \times 10^{-5}$–$17.32$, and $Ste = 0.0444$–0.385. The effects of water velocity and water temperature on the melting and heat transfer in the melting process are analyzed. The effects of packing patterns on Nusselt number correlations are presented. Using the definition of a terminal velocity, a Reynolds number ratio is developed as the criterion defining the floating, non-floating or transitional packing pattern.

Keywords: Packed bed; Melting; Phase change; Convection; Heat transfer

1. Introduction

Packed bed processes with melting of the solid particles are found in materials processing and heat transfer operations in various industries and also occur in the environment. For example, solid materials are poured into molten materials in smelting operations, alloying operations, and vitrification processes for materials production and destruction of hazardous waste. Transport phenomena of packed particles with phase change and liquid play important roles not only for achieving the stable operation of these processes but also for improving the operating efficiency. In a natural environment, an ice jam in a river is an example of melting of a packed bed of solid subject to a flowing liquid. To avoid a sudden release of water as a result of melting of an ice jam in a river, or malfunction of frozen water pipes, accurate prediction of ice–water flow is required [1]. In the food processing industry, application of ice slurry transport for food production requires the two-phase flow to be pumped through a piping system over a distance. The accurate determination of heat loss associated with melting is required to allow the design of more efficient systems. To achieve this, proper design tools such as average heat transfer coefficient of a melting slurry flow are needed. The same observation holds for phase change material (PCM) applied to convective heat exchangers. Strictly speaking, the packed bed defined in this paper is slightly relaxed because in some cases, the particles may be locally dispersed but far from the state of fluidized bed. From practical point of view, it is proper to use the packed bed concept for discussion in this paper.

For a melting packed bed subject to a flow, the incoming fluid is often not at the same temperature as the melting particles. This causes a non-thermal equilibrium between the flowing fluid and melting solid particles. Heat transfer characteristics are therefore influenced by three distinctive, yet related convective mechanisms:

* Corresponding author. Tel.: +1-305-348-3015; fax: +1-305-348-1932.
E-mail address: taoy@fiu.edu (Y.-X. Tao).

0017-9310/$ - see front matter © 2003 Elsevier Ltd. All rights reserved.
doi:10.1016/S0017-9310(03)00359-4

Nomenclature

c_p	specific heat, J/(kg °C)
$\bar{d}_V$	average volume diameter, m
Gr	Grashof number, $g_0\beta_{l0}\rho_{l0}^2\bar{d}_V^3(T_{l0}-T_m)/\mu_{l0}^2$
g	gravitational acceleration, m/s^2
h	heat transfer coefficient, W/(m^2 °C)
h_{ls}	latent heat of fusion, J/kg
k	thermal conductivity of water, W/(m °C)
M_s	mass of ice particles in packed bed, kg
$\dot{m}_s$	total melting rate of ice particles, kg/s
$\dot{m}_s'$	average melting rate per unit bed volume, kg/(m^3 s)
N	number of ice particles in the packed bed
Nu	local Nusselt number, $h\bar{d}_V/k_{l0}$
Pr	Prandtl number, $\mu_{l0}c_{pl0}/k_{l0}$
q	heat transfer rate, W
R	outside radius of ice sphere, m
Re	Reynolds number, $\rho_{l0}v_{l0}\bar{d}_V/\mu_{l0}$
r	radius coordinate inside ice, m
S	surface area of particles per unit volume, m^{-1}
Ste	Stefan number, $c_{pl0}(T_{l0}-T_m)/h_{ls}$
T	temperature, °C
t	time, s
t^*	dimensionless time
v_l	water velocity, m/s
V	volume, m^3

Greek symbols

α	thermal diffusivity, m^2/s
β	coefficient of thermal expansion, K^{-1}
μ	viscosity, Pa s
ρ	density of ice, kg/m^3
ε	volume fraction

Subscripts

0	at the inlet; initial
B	packed bed
l	liquid, water
m	phase change
s	solid, ice

Other

– (overbar) averaged

(1) complex interstitial (interparticle) flow pattern due to discharge of melt and non-thermal equilibrium fluid mixing with the supply fluid;
(2) packing pattern as a result of non-zero relative velocity between particles and fluid, which results from melting and phase density buoyancy; and
(3) bypass flow between the packed bed and liquid only flow region, resulting from reduction of total bed volume due to melting.

Fig. 1(a) illustrates those three main mechanisms where the adiabatic boundary condition for the flow passage wall is imposed. For other boundary conditions where heat transfer through the passage wall is not negligible, in some cases even dominant, the transport phenomena become even more complicated.

In the literature, very limited efforts have been devoted in addressing convective melting and related heat transfer characteristics. Kearns and Plumb [2] studied experimentally the contact melting of a packed bed. Tao and coworkers [3,4] presented the experimental observations and results for melting of a single ice particle in a non-thermal equilibrium flow. Plumb [5] presented a numerical analysis of convective melting of packed beds. In his analysis, thermal non-equilibrium is considered, but the granular motion is neglected. The very limited motion of the particles was allowed in their later work [6]. They adopted the constant porosity model and the constant volume model to prescribe the motion process of the packed bed. Sabau and Tao [7] proposed a model to predict the melting characteristics during one- and two-dimensional convective melting processes for a packed bed. Jiang et al. [8] developed a numerical modeling of two-dimensional convective melting of granular packed beds based on Sabau and Tao's work [7]. They divided the entire computational domain into two subdomains, the pure fluid and the melting packed bed. The single-phase model and two-phase model was used for two subdomains, respectively. In their model, it is assumed that the packed bed maintains a uniform porosity.

In Part II of this study [9], we will present the numerical results for a three-dimensional model of two-phase flow and heat-mass transfer with phase change, based on the theory of interacting continua. The model considers such effects as relative motion between particles and fluid, non-thermal equilibrium between solid and liquid, and time variation of phase volume fractions from which repacking of the packed bed can be derived. Such a numerical tool will aid in design of a thermal system where fluid and melting packed beds are encountered. For this purpose, we design a benchmark experiment to study heat transfer characteristics involving convective melting for a horizontal flow. We focus on a process where solid particles are the same species as the liquid, an ice–water system. The reason why the horizontal configuration is studied is to develop the predictability for multi-dimensional, complex physical phenomena that are encountered in real applications that one-dimensional studies such as [3,7] could not

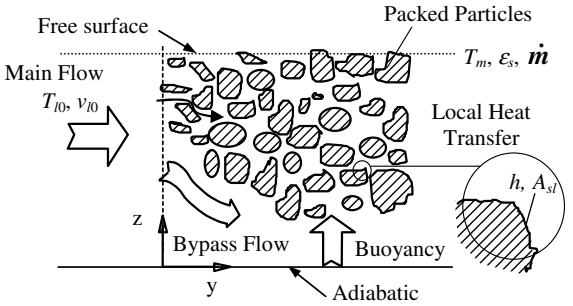

(a)

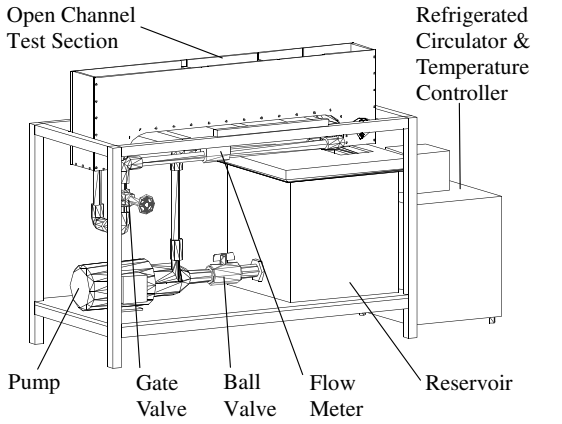

(b)

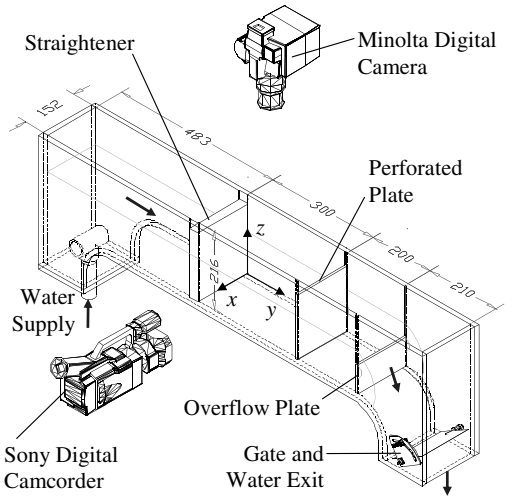

(c)

Fig. 1. (a) Flow and heat transfer characteristics of a melting packed bed subject to a horizontal main flow at a non-equilibrium temperature; (b) schematic of the test apparatus; (c) test section and cameras setup.

accomplish. In some material processing applications, melting particles may have a higher density than its liquid phase has. In addition, water density inversion at 4 °C does not bear similarity with other materials; therefore, the reader should be cautious when the results reported in this study are to be extrapolated to other materials applications.

2. Experiments

2.1. Apparatus

The experimental setup shown in Fig. 1(b) is used to investigate the convective melting of a packed bed in the horizontally flowing water. The test facility consists of a closed and forced circulation loop of water and a temperature controlled circulation loop. A MARCH TE-7R-MD pump moves water from the reservoir and discharges it to the constant head tank, from which the water flows into the channel. Water flows downstream in the channel through the packed bed of ice particles, which is held in the test section by a perforated stop plate at downstream, and is then routed back to the reservoir. The discharge line has a gate valve and a John C. Ernst Co S100 flow meter to control and measure the flow rate of water. Water temperature is controlled by a refrigerated circulator with a measured fluctuation of 0.1 °C during a typical experiment.

The test section is the middle part of the open channel, shown in Fig. 1(c). The length, width, and height of the test section are 300, 152, and 216 mm, respectively. A uniform velocity at the inlet of the test section is attained by the use of a flow straightener made of Duocel aluminum foam. An overflow plate placed at the downstream location controls the water level. Alternatively, a gate placed at the exit location can also control the flow level. The channel is made of Plexiglas so that experiments could be visualized and videotaped. A Sony digital camcorder is used to continuously record the image from the side view. A Minolta digital camera is used to intermittently take the pictures from the top view. Fifteen thermocouples are mounted at the inlet, exit and in the test section so that the water and bed temperature at different locations along the flow direction can be measured. A computer with OMEGA DAS-TC/B data acquisition system is used to record the thermocouples readings during tests. To measure the distribution of water temperature at the exit cross-section, nine thermocouples in a 3×3 matrix are mounted on the backside of the perforated plate. The distances of three rows to the bottom of the test section (in z-direction, Fig. 1(c)) are 35, 65, and 85 mm, respectively. The distances of three columns to the backside of the test section (in x-direction, Fig. 1(c)) are 39, 80, and 120 mm, respectively. To avoid touching the particles and to measure the liquid temperature only, each pair of thermocouples is mounted on the backside (right side on

Fig. 1(c)) of the perforated plate and at the center of a corresponding through-hole.

The packed bed is composed of hemispherical ice particles, which are made and stored in a freezer. The initial volume diameter of ice particle is 26.2 mm. The volume diameter is defined as the diameter of an equivalent sphere having the same volume as the particle. The freezer is also used to control the initial temperature of ice particles. A special basket with the same size as the test section is made of stainless steel wire and fine nylon screen to measure the mass change of the packed bed during the melting process. With the basket, the ice particles that compose the packed bed can be removed from the test section; therefore, the total mass of packed bed at a desired time can be determined by weighing on an electronic scale.

2.2. Experimental procedure

During a typical test, the pump is turned on first. A steady open channel flow at the desired flow rate and temperature is established by adjusting a control valve and setting the refrigerated circulator. The digital video camcorder and the computer data acquisition system then start to record the video images and the temperatures. The basket that contains an initial ice mass at the desired initial temperature and stored in the freezer before the test is placed in the test section, which marks the beginning of a test. After a desired time interval, the basket with the ice packed bed is removed from the test section, dried, and reweighed. The mass of particles at that time is determined from the total weight subtracting the weight of the basket. The procedure is repeated under the same condition for different time intervals. After each test is completed, the shape of the packed bed can be obtained from the digital video images by using a standard image analysis software. The accuracy of the dimension measurements is ±0.2 mm. The volume of the packed bed is determined by numerical integration.

2.3. Data processing

The volume of ice particles in the packed bed is determined as follows:

$$V_s = \frac{M_s}{\rho_s}. \tag{1}$$

The average volume fraction of ice particles in the packed bed is defined as

$$\bar{\varepsilon}_s = \frac{V_s}{V_B}. \tag{2}$$

The melting rate of ice particles in the packed bed can be determined from the variation of the mass with time as follows:

$$\dot{m}_s = -\frac{\Delta M_s}{\Delta t}. \tag{3}$$

The average melting rate per unit bed volume is

$$\bar{\dot{m}}'_s = \frac{\dot{m}_s}{V_B}. \tag{4}$$

The average heat transfer coefficient can be defined based on the interfacial energy balance. The heat transferred from the water to the ice surface must be equal to the sum of the latent heat required to melt the ice at the rate $\dot{m}_s$ and the conduction of heat from the ice surface to the inside, when the inside of ice is at a temperature lower than the melting temperature T_m (0 °C). Therefore, we have

$$\bar{h} = \frac{\dot{m}_s h_{ls} + q_{in}}{V_B \overline{S}_B (T_{l0} - T_m)}, \tag{5}$$

where $\overline{S}_B$ is the surface area of particles per unit bed volume, defined as

$$\overline{S}_B = \frac{6\bar{\varepsilon}_s}{\bar{d}_V}, \tag{6}$$

and $\bar{d}_V$ is the average diameter of equivalent spherical particles based on the volume of ice particles in the packed bed, which can be determined according to the measurement results of ice mass in the packed bed,

$$\bar{d}_V = \sqrt[3]{\frac{6M_s}{\pi N \rho_s}}, \tag{7}$$

where N is the number of ice particles in the packed bed determined experimentally.

The experimental determination of the conduction heat rate q_{in} in Eq. (5) is difficult. As an approximation, we determine its value by solving the heat conduction equation under the assumptions that the ice particles keep the spherical shape and are homogeneous during the melting process. The typical ice particle in the packed bed can be described approximately as an ice sphere of initial radius R_0 having the uniform initial temperature T_{s0} and being plunged suddenly into a bath at temperature T_{l0}. The surface temperature of ice is at the melting temperature T_m. The mathematical solution for $\theta_s = T_s - T_m$ and conduction rate for each particle $q(t_i)$ can be derived from [10]. The conduction heat rate q_{in} at time t_i in Eq. (5) is given as

$$q_{in} = Nq(t_i). \tag{8}$$

2.4. Experimental uncertainty

Single-sample uncertainties for the present study were estimated using the method of Kline and McClintock [11]. The primary measurements in the present study are flow rate of water, mass of ice particle in the

packed bed, time, temperatures, dimension and locations. The maximum random uncertainty in the flow rate was estimated as ±2.0%. For mass it was ±0.002 kg. The maximum random uncertainty in the time, which was recorded by data acquisition, was estimated as ±0.5 s. For temperature and dimension, the maximum random uncertainty was ±0.5 °C and ±0.2 mm, respectively. Taking into account the uncertainties in mass, time, and volume, the maximum uncertainty in the average melting rate per unit bed volume is estimated to be less than ±4.23%. For the volume fraction, considering the uncertainty in volume, the maximum uncertainty is less than ±8.0%. For heat transfer coefficient with the uncertainties in melting rate, volume, volume fraction and temperature, its maximum uncertainty is less than ±7.69%. To estimate the repeatability of the experiment, some of cases were repeated under the same operating conditions. The difference was found less than 3%.

3. Results and discussion

Experiments were carried out for different supply water velocities and temperatures. The dimensionless time, defined as the ratio of time to total melting time, $t^* = t/t_{\text{total}}$, is used to present temporal results in this study. It should be pointed out that the total time from the start to the time when all ice particles in the packed bed is melt is different under different test conditions. The actual total time is also listed in the description of results for the quantitative comparison. The volume of packed bed and mass of ice particles in the packed bed are also different for the same dimensionless time but under different test conditions. Therefore, the average melting rate per unit bed volume is used to quantify the melting process in the present study.

3.1. Average melting rate per unit bed volume

3.1.1. Effect of velocity

Fig. 2(a) shows the variation of average melting rate per unit bed volume $\bar{\dot{m}}_s'$ with time for different water velocities. Three cases with the inlet water velocity of 0.01, 0.05, and 0.10 m/s, respectively, are conducted while keeping the inlet water temperature at 30 °C, the initial ice temperature at −20 °C, and the initial ice mass at 2 kg. It is obvious that the higher water velocity enhances the transport of energy and mass between water and ice particles, causing the ice particles to melt faster. In the meantime, the drag force exerted by the water flow increases with the velocity, causing the ice particles to repack more tightly. The average volume fraction of ice particles $\bar{\varepsilon}_s$ increases. It can be seen in Fig. 2(b) that the value of $\bar{\varepsilon}_s$ in the case of $v_{l0} = 0.10$ m/s is greater than the ones in the cases of $v_{l0} = 0.01$ and 0.05 m/s. The increase in the volume fraction of ice particles results in the increase in the surface area per unit bed volume $\overline{S}_B$. Fig. 2(c) shows that the value of $\overline{S}_B$ in the case of $v_{l0} = 0.10$ m/s is greater than those values in the cases of $v_{l0} = 0.01$ and 0.05 m/s. High values of surface area per unit bed volume could be favorable for the melting. However, the effect of buoyancy on the packing pattern of the bed becomes significant when the velocity is small.

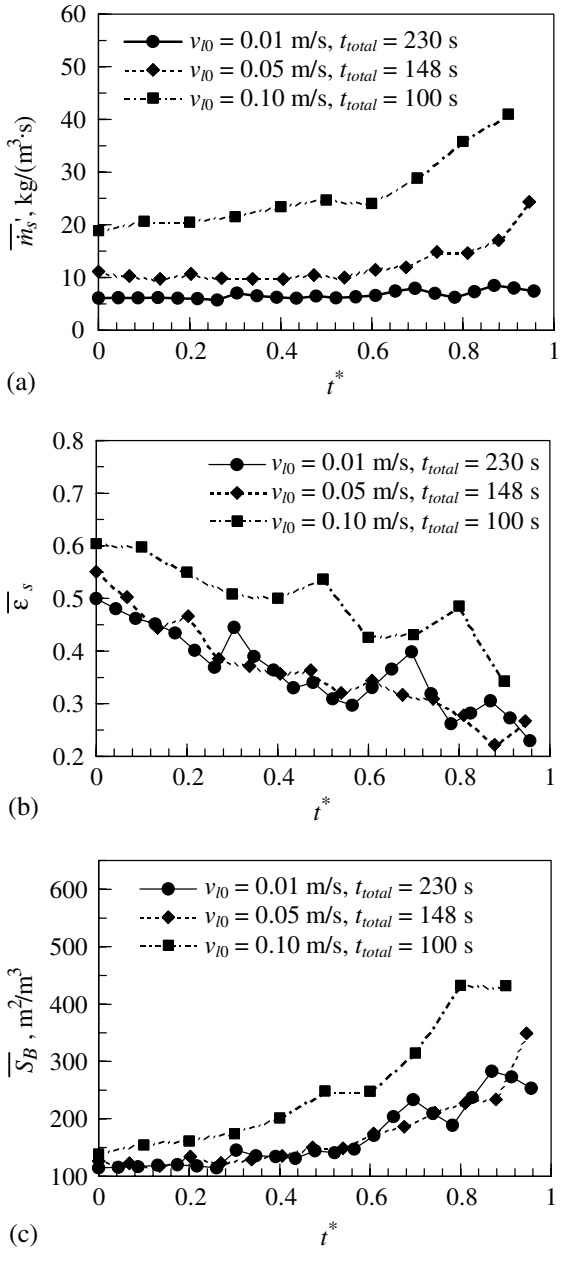

Fig. 2. Time variation of (a) melting rate per unit bed volume, (b) volume fraction of ice particles, and (c) surface area per unit bed volume for different water velocities: $T_{l0} = 30$ °C, $T_{s0} = -20$ °C, $d_{V0} = 26.2$ mm, $M_{s0} = 2$ kg.

The difference in the packing pattern of the bed between the cases of $v_{l0} = 0.01$ and 0.05 m/s is not very obvious in Fig. 2(a) and (b).

The results also indicate that the melting rate per unit bed volume $\bar{m}'_s$ increases with the time in the melting process. It is because the sizes of ice particles decrease along with the melting causing the increase in the surface area per unit volume $\overline{S}_B$ (see Eq. (6)). This can be demonstrated by the ratio of surface area to volume for a sphere, which equals $3/R$. Fig. 2(c) shows this trend. However, the average volume fraction of ice particles $\bar{\varepsilon}_s$ decreases with time, as shown in Fig. 2(b), which is because there is enough space for ice particles to float up to the surface of water and loosely pack as the size and number of ice particles decrease. The decrease in the average volume fraction of ice particles $\bar{\varepsilon}_s$ could partly hinder the increase in the surface area per unit volume $\overline{S}_B$.

The packing pattern of the bed keeps changing while the ice particles are melting and moving. Because the aggregation between the particles occurs randomly, some of particles cannot move smoothly and pack evenly. Strong repacking occurs when some or all of the aggregated particles are released. Those phenomena cause step-jump changes in volume fraction and surface area per unit bed volume, as observed at the several points in Fig. 2(b) and (c). This should explain why the variation of average melting rate per unit bed volume with time is not very smooth, as shown in Fig. 2(a).

3.1.2. Effect of temperature

Fig. 3(a) shows the variation of average melting rate per unit bed volume $\bar{m}'_s$ with time for different water temperatures. Four cases are conducted for the inlet water temperature of 4, 10, 20, and 30 °C, respectively while keeping the inlet water velocity at 0.1 m/s, the initial ice temperature at −20 °C, and the initial ice mass at 2 kg. The results indicate that higher water temperature causes the increase in the average melting rate per unit bed volume. The increase in heat transfer is an obvious reason as the temperature difference increases. On the other hand, the values of $\bar{\varepsilon}_s$ in the higher water temperature cases are greater than those in the lower temperature cases except for the case of $T_{l0} = 4$ °C, as shown in Fig. 3(b). The higher the value of $\bar{\varepsilon}_s$, the higher the value of $\overline{S}_B$ is, as shown in Fig. 3(c). This again results from the enhanced transports of heat and mass between water and ice particles.

The case of $T_{l0} = 4$ °C displays a special phenomenon comparing with the other cases, as shown in Fig. 3(b). The density of mainstream water reaches the greatest value at 4 °C due to the density inversion. The buoyancy due to the density difference between water and ice particles also reaches the peak value at 4 °C causing tighter particle packing. The density of mainstream flow in the lower region is even greater than the densities of melt from ice particles in the bed region. Under this condition, thermal natural convection in the vertical direction, which would otherwise loosen up the ice particles, has little effect to the interstitial flow. These effects result in a higher value of $\bar{\varepsilon}_s$ for $T_{l0} = 4$ °C and its trend different from the other cases. Also observed in this case, the value of $\bar{\varepsilon}_s$ approximately approach a constant at the later stage of the melting process, and $\bar{m}'_s$

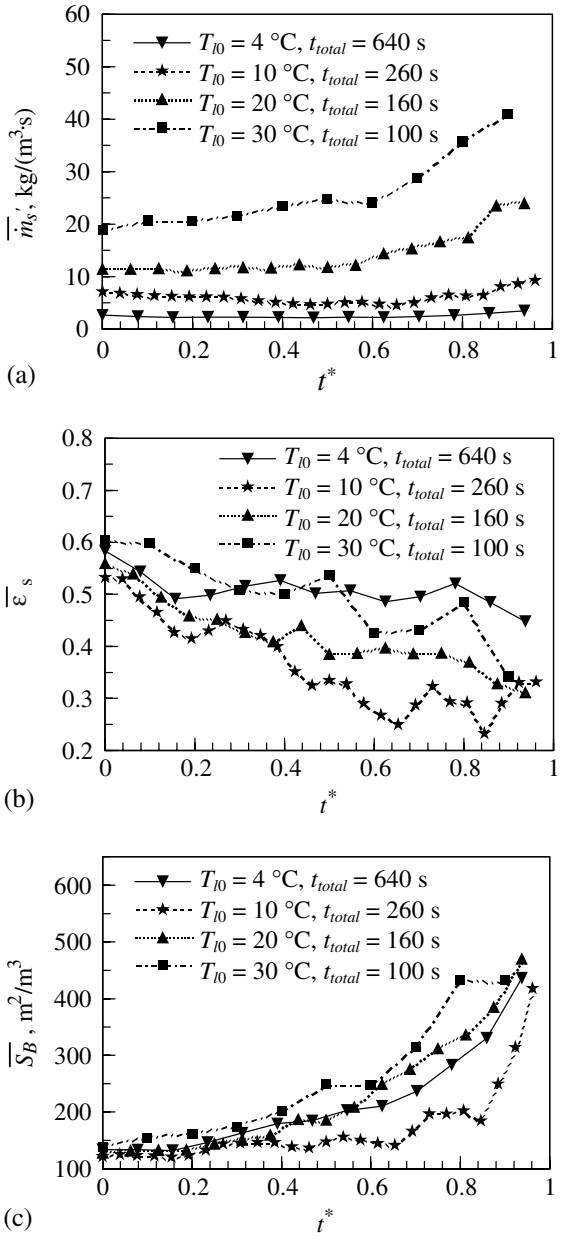

Fig. 3. Time variation of (a) melting rate per unit bed volume, (b) volume fraction of ice particles, and (c) surface area per unit bed volume for different water temperatures: $v_{l0} = 0.10$ m/s, $T_{s0} = -20$ °C, $d_{V0} = 26.2$ mm, $M_{s0} = 2$ kg.

becomes the lowest in Fig. 3(a) because the temperature difference between water and ice particles is the smallest, even though the values of $\bar{\varepsilon}_s$ and $\overline{S}_B$ are greater than in Fig. 3(b) and (c).

Another interesting observation is that a high melting rate per unit bed volume corresponds a high volume fraction of ice particles, as shown in Fig. 2(a) and (b), and Fig. 3(a) and (b). One possible reason is that increased volume of melt from ice particles enhances lubrication effect between the ice particles, which keeps remaining ice particles from sticking and blocking. Therefore, particles move more smoothly, and packing becomes tighter.

Figs. 2(b) and 3(b) illustrate that the average volume fraction of ice particles decreases with the elapse of time. It is obvious that to model such a complex transport phenomenon one cannot assume the bed kept at a constant porosity or constant volume as suggested in the literature [5].

3.2. Packing pattern of melting packed bed

The geometric change and buoyancy make the packing pattern (a non-uniform redistribution of solid volume fraction) and repacking phenomena of melting particles in a horizontal flowing fluid much more complex than that in regular packed bed. In general, the packing pattern is governed by flow strength, properties of fluid and particle, and geometric characteristics of particles and channel. Figs. 4 and 5 show two typical packing patterns during the melting process, in which water flows from the left side to the right side in the figures.

A general packing pattern starts to form when the test section is initially full of ice particles in water flow. The melting ice particles float to the upper surface since the density of ice is less than that of water, and are pushed towards downstream to form the packed bed. Because of melting the volume of ice particles decreases. Due to the drag forces that are exerted by water flow on ice particles and the buoyancy force, non-sticking particles are forced to move downstream and upwards to repack continuously. The different packing patterns appear under the different conditions of flow while melting is in process. The remaining ice particles float to the upper surface and form a floating packed bed when flow velocity is low, as shown in Fig. 4. On the other hand, if the velocity is high enough (shown in Fig. 5), the remaining ice particles are pushed to the perforated plate and form a packed bed against the plate. We call them the floating packed bed and the non-floating packed bed, respectively.

Figs. 6 and 7 show the variations of liquid temperature distribution at the outlet of the test section with time for the two cases shown in Figs. 4 and 5, respectively. They clearly show the basic difference between the two types of packed beds. As melting continues, the horizontal linear dimension of the bed gradually decreases from the top surface to the bottom, as shown in Figs. 4 and 5. The water temperature decreases as it flows through the packed bed and exchanges energy with the ice particles through combined conduction and convection including mixing with discharged melt. The water temperature decreases further when flow undergoes a longer path through the packed bed. Therefore, the temperature in the upper region is lower than that in the lower region, as shown in Figs. 6(a) and 7(a).

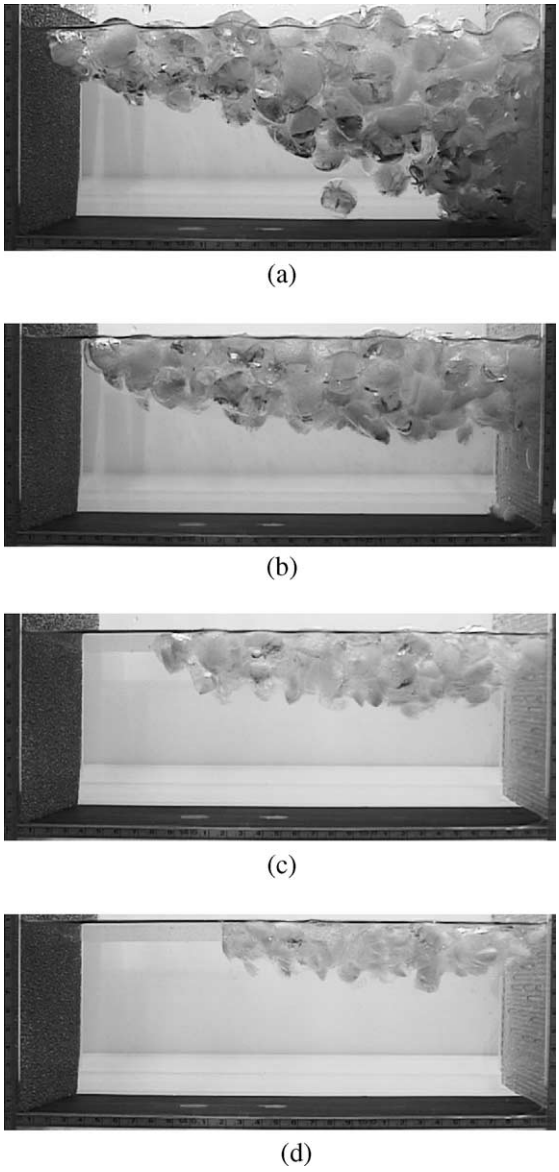

Fig. 4. Typical floating packed bed: $v_{l0} = 0.07$ m/s, $T_{l0} = 30$ °C, $T_{s0} = 25$ °C, $d_{V0} = 26.2$ mm, $M_{s0} = 2$ kg, $t_{total} = 140$ s. (a) $t = 10$ s, $t^* = 0.071$. (b) $t = 30$ s, $t^* = 0.214$. (c) $t = 50$ s, $t^* = 0.357$. (d) $t = 70$ s, $t^* = 0.5$.

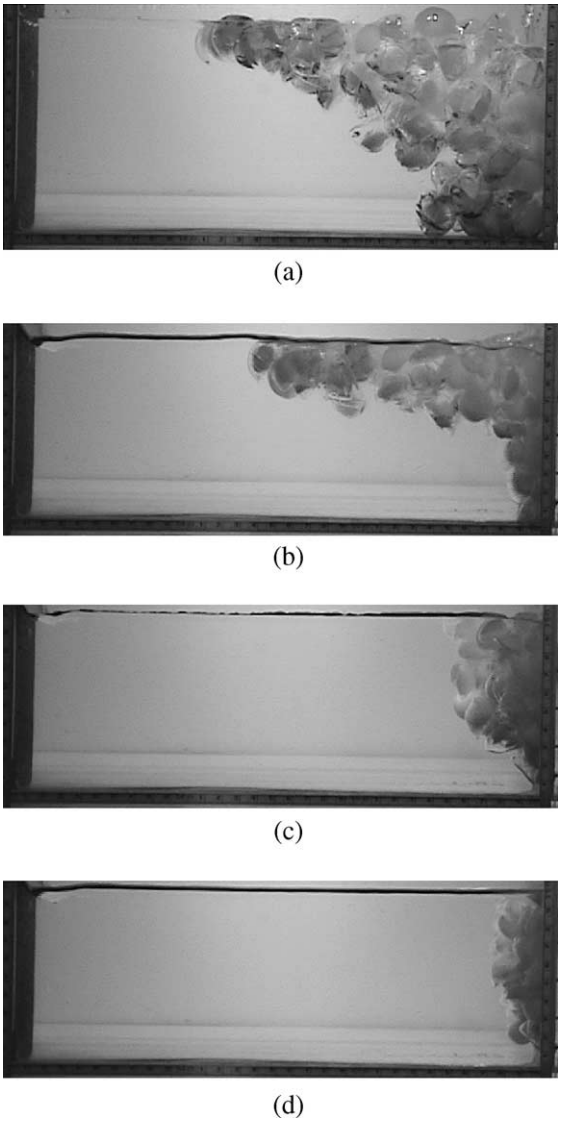

Fig. 5. Typical non-floating packed bed: $v_{l0} = 0.13$ m/s, $T_{l0} = 10$ °C, $T_{s0} = 20$ °C, $d_{V0} = 26.2$ mm, $M_{s0} = 1.0$ kg, $t_{total} = 110$ s. (a) $t = 10$ s, $t^* = 0.091$. (b) $t = 30$ s, $t^* = 0.273$. (c) $t = 50$ s, $t^* = 0.455$. (d) $t = 60$ s, $t^* = 0.545$.

For the floating packed bed (Fig. 4), the liquid temperature increases in the lower region while the melting continues, and remaining ice is repacking in the upper region. The liquid bypasses the packed bed in the lower region without in contact with ice particles, and the temperature is almost the same as the inlet temperature, as shown in Fig. 6(c)–(f). The bypass region increases with time; therefore, the contact between the flow and ice particles is even less.

For the non-floating packed bed (Fig. 5), the region where the liquid temperature is lower than the inlet temperature is much larger than that in the floating packed bed, as shown in Fig. 7. The majority portion of the outlet cross-section is very much covered by melting packed bed even at $t^* = 0.727$ when the melting process is almost finished, as shown in Fig. 7(f). The non-uniform temperature variation in Fig. 7 also shows that strong repacking occurs during the melting process. The ice particles are pushed to downstream against the perforated plate while floating up. That is the reason why the low temperature region may be increased downwards during the melting process; i.e., the low temperature area in Fig. 7(f) is greater than in Fig. 7(e). The above temperature results clearly show that in the non-floating packed bed, heat transfer is enhanced for the water flows through the packed bed with effective contact between the flow and particles.

All of the results that we present in Section 3.1 (Figs. 2 and 3) are under the condition of floating packed beds. Fig. 8(a) shows the variation of average melting rate per unit bed volume $\bar{\dot{m}}'_s$ with time for different water velocities in the typical floating and non-floating packed beds. Three cases for the different inlet water velocity of 0.05, 0.10, and 0.13 m/s, respectively, are presented. The cases of $v_{l0} = 0.05$ and 0.10 m/s are for typical floating packed beds, in which features of melting are similar to those cases discussed in Section 3.1. The case of $v_{l0} = 0.13$ m/s is for a typical non-floating packed bed, in which the melting characteristics are significantly different from the floating bed cases. The value of $\bar{\dot{m}}'_s$ in the non-floating packed bed is much higher than that in the floating ones. For example, doubling the flow velocity from 0.05 to 0.10 m/s results in a mere doubling in the $\bar{\dot{m}}'_s$ value for the floating packed bed. The only 30% increase in velocity from 0.1 to 0.13 m/s causes multiple-folds increase in $\bar{\dot{m}}'_s$ when the packed bed changes from floating packing pattern to the non-floating packing pattern, as shown in Fig. 8(a). Obviously, the velocities in the non-floating cases are higher than that in the floating cases because the non-floating packing only occurs under the condition of relative high velocity. However, this is not the only reason. As discussed above, another important reason that influences the melting characteristics is the change of packing pattern. The interaction between the liquid flow and particles in the non-floating packed bed is much more effective than in the floating packed bed. Fig. 8(b) indicates that the particles are pushed to downstream against the perforated plate forming a tighter, non-floating packed bed. The value of $\bar{\varepsilon}_s$ in the case of 0.13 m/s is almost constant and higher than the floating bed cases during the melting process.

3.3. Average heat transfer coefficient

Heat transferred from water to the ice particles can be divided into two parts: one is the latent heat for fusion on the surface, and the other is conduction heat

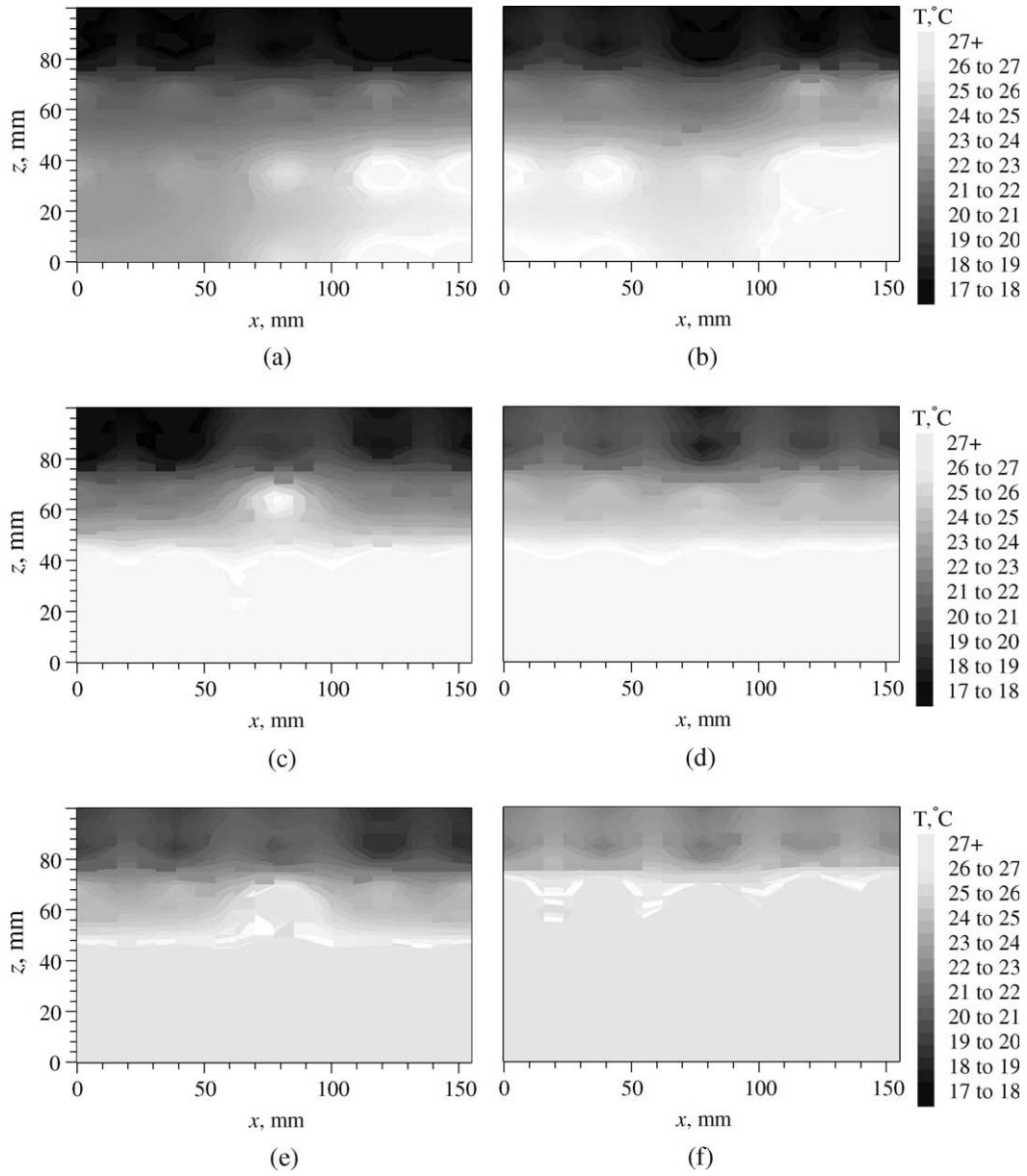

Fig. 6. Typical time variation of temperature distribution at the outlet: the same condition as in Fig. 4. (a) $t = 10$ s, $t^* = 0.071$. (b) $t = 13$ s, $t^* = 0.093$. (c) $t = 23$ s, $t^* = 0.164$. (d) $t = 33$ s, $t^* = 0.236$. (e) $t = 43$ s, $t^* = 0.307$. (f) $t = 66$ s, $t^* = 0.471$.

from the surface into the inside of ice to raise the internal temperature. The internal temperature of the particles is lower than the surface temperature, the melting temperature, in the early period of melting process. The value and effective duration of conduction heat depend on the initial temperature, size and shape of ice particles. The effective duration for the internal particle temperature to reach the melting temperature is much shorter than that without melting because the melting on the surface causes the particle radius to decrease. Fig. 9 shows a typical time variation of latent heat rate for fusion, the conduction heat rate, and the total heat transfer rate from water to ice particles. It can be seen that the effect of heat conduction can be neglected after 30 s in the case shown.

3.3.1. Effect of velocity

Fig. 10(a) shows the variation of average heat transfer coefficient $\bar{h}$ with time for three cases shown in Fig. 2. It can be seen that $\bar{h}$ for the high velocities is

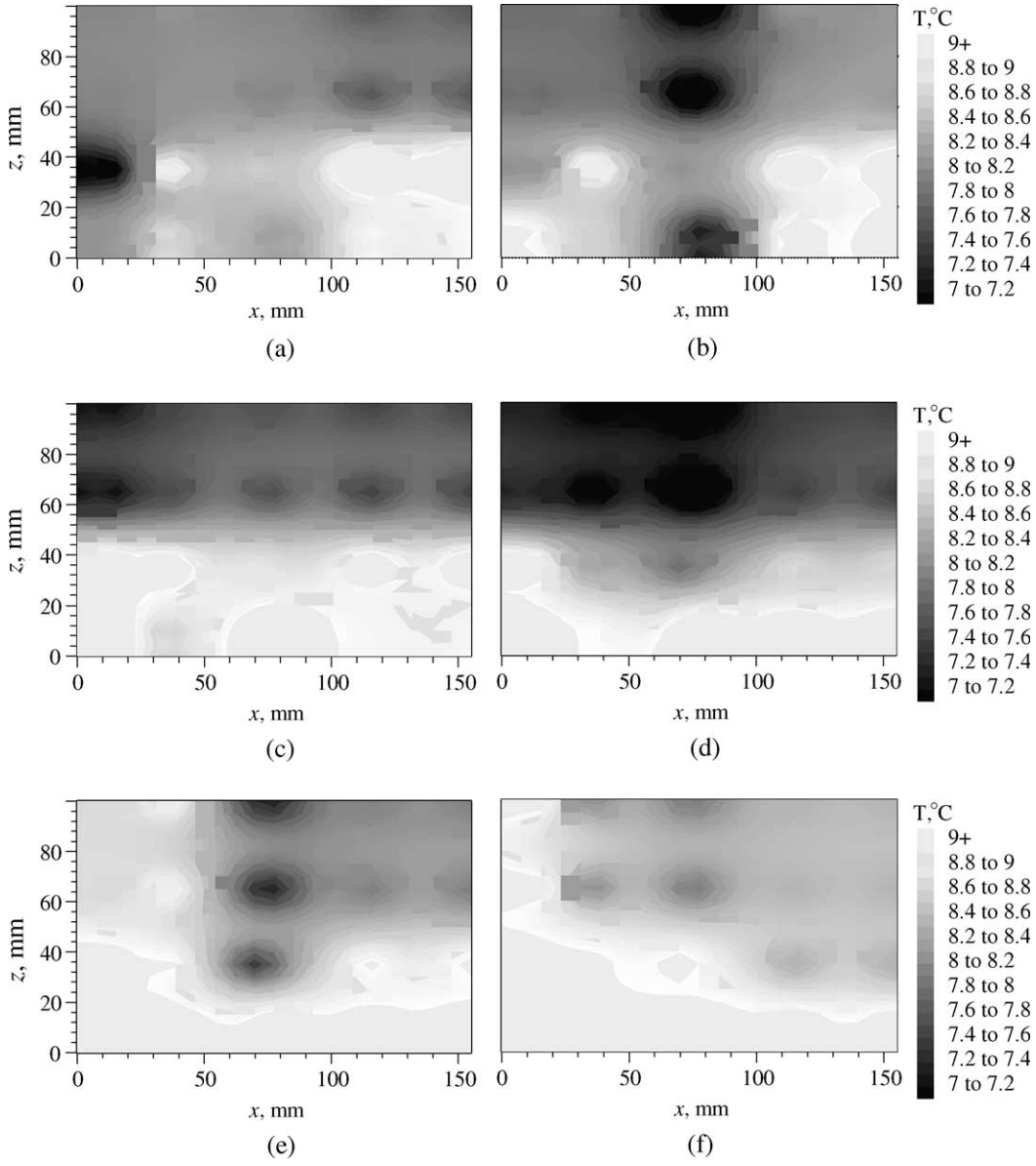

Fig. 7. Typical time variation of temperature distribution at the outlet: the same condition as in Fig. 5. (a) $t = 20$ s, $t^* = 0.182$. (b) $t = 30$ s, $t^* = 0.273$. (c) $t = 40$ s, $t^* = 0.364$. (d) $t = 50$ s, $t^* = 0.455$. (e) $t = 70$ s, $t^* = 0.636$. (f) $t = 80$ s, $t^* = 0.727$.

greater than that of lower velocities. In general, the value of $\bar{h}$ decreases with the elapse of time in the melting process although $\bar{m}'_s$ increases, comparing Figs. 10(a) and 2(a). This trend is opposite to that in the melting process of a single ice particle in a flow [4], where the average heat transfer coefficient actually increases with time because the size of particle decreases, causing the decrease in the boundary-layer thickness and hence the decrease in the resistance to heat transfer. In the packed bed, the flow pattern in the void between the particles mainly influences the heat transfer. The decrease in $\bar{\varepsilon}_s$ in the melting process (shown in Fig. 2(b)) indicates that the ice particles are packing loosely while melting continues. It would cause water through the packed bed to flow slowly and smoothly so that $\bar{h}$ decreases. Although $\bar{h}$ decreases, $\bar{m}'_s$ still increases as mentioned above because of the increase in $\overline{S}_B$ (Figs. 2(c) and 3(c)).

3.3.2. Effect of temperature

Fig. 10(b) shows the variation of average heat transfer coefficient $\bar{h}$ with time for the cases shown in Fig. 3, which are at different water temperatures. The

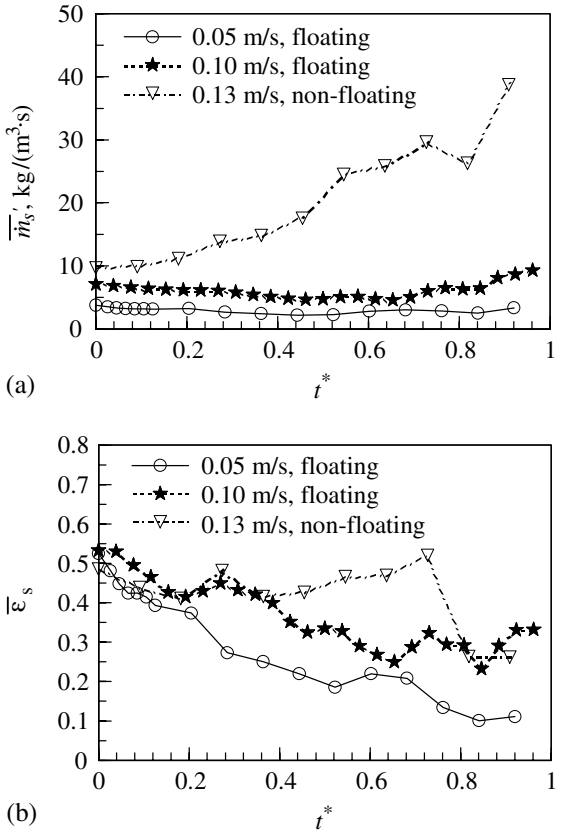

Fig. 8. Time variation of (a) melting rate per unit bed volume and (b) volume fraction of ice particles for different water velocities: $T_{l0} = 10$ °C, $T_{s0} = -20$ °C, $d_{V0} = 26.2$ mm, $M_{s0} = 2$ kg.

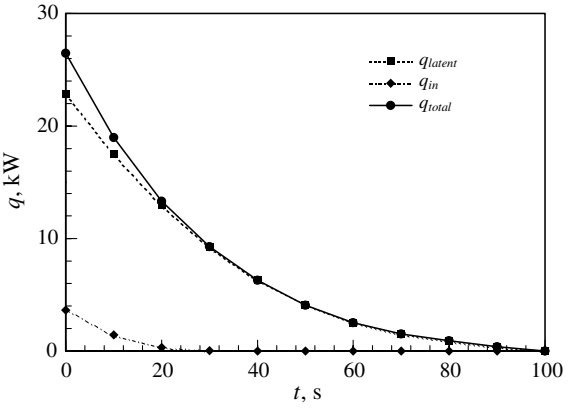

Fig. 9. Typical time variation of latent heat rate for fusion, conduction heat rate from ice surface to inside, and heat transfer rate from water to ice particles in the melting process: $v_{l0} = 0.10$ m/s, $T_{l0} = 30$ °C, $T_{s0} = -20$ °C, $d_{V0} = 26.2$ mm, $M_{s0} = 2$ kg.

trend is similar to Fig. 10(a), i.e., the value of $\bar{h}$ decreases with the elapse of time. The variation of water temperature mainly affects the thermal properties besides the temperature difference between water and ice particles. The effect of water temperature on the average heat transfer coefficient is not remarkable, as in the cases of $T_{l0} = 10$, 20, and 30 °C shown in Fig. 10(b). In the special case of $T_{l0} = 4$ °C, the density of mainstream water is greater than the density of melt from ice particles. The melt cannot move downwards because of the density difference, causing a weak cross-flow in the packed bed. Therefore, $\bar{h}$ in the case of $T_{l0} = 4$ °C is slightly lower than that in other cases.

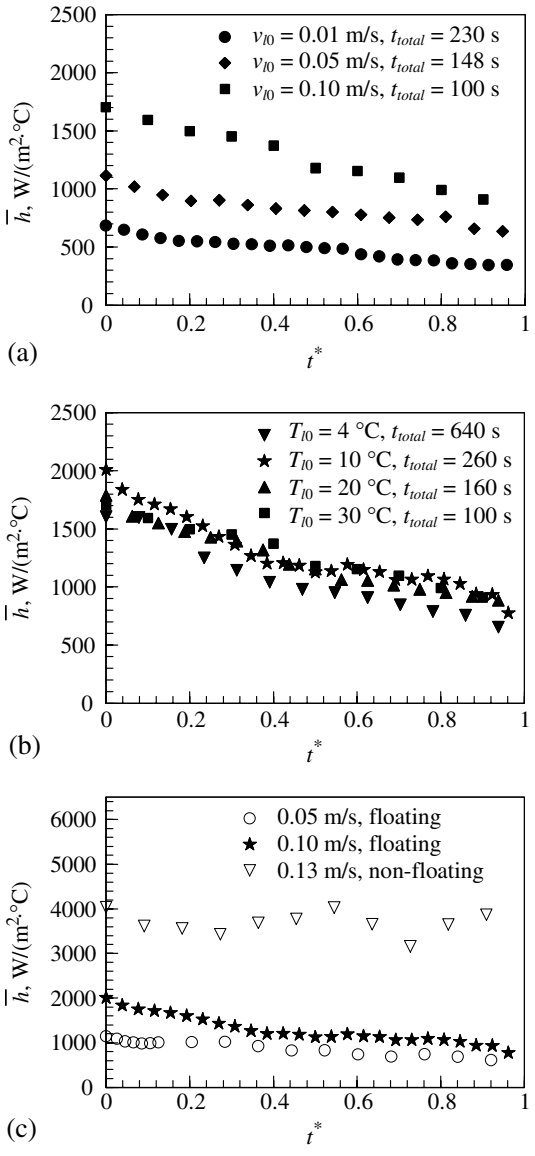

Fig. 10. Time variation of average heat transfer coefficient for (a) different water velocities ($T_{l0} = 30$ °C), (b) different water temperatures ($v_{l0} = 0.10$ m/s), and (c) different water velocities ($T_{l0} = 10$ °C): $T_{s0} = -20$ °C, $d_{V0} = 26.2$ mm, $M_{s0} = 2$ kg.

3.3.3. Effect of packing pattern

Fig. 10(c) indicates the significant difference in heat transfer characteristics between the floating and non-floating packed beds. The conditions in Fig. 10(c) are the same as those in Fig. 8. Heat transfer is more effective in a packed bed with non-floating packing pattern because of better interaction between main flow and individual particles. Therefore, the heat transfer coefficient in the non-floating packed bed is higher and almost constant, as shown in Fig. 10(c). The 100% increase in velocity from 0.05 to 0.10 m/s results in a mere doubling in $\bar{h}$ value for the floating packed bed. The only 30% increase in velocity from 0.1 to 0.13 m/s causes more than 200% increase in $\bar{h}$ when the packed bed changes from the float-packing pattern to the non-floating packing pattern.

3.4. Correlations for Nusselt number

As discussed above, there is remarkable difference in heat transfer characteristics in the two types of packing patterns. Accordingly, using a regression analysis two correlations for the average heat transfer coefficient are obtained in this study.

The empirical correlation for the average heat transfer coefficient between the flow and melting particles in the non-floating packed bed is obtained as follows:

$$Nu = 2 + 2.56 \times 10^{-4} Re^{1.43} Pr^{1/3} Ste^{-0.66}, \quad (9)$$

which is valid for

$304 \leqslant Re \leqslant 1996$, $0.000151 \leqslant Gr/Re^2 \leqslant 0.00443$, and $0.0444 \leqslant Ste \leqslant 0.128$.

An R^2 value for Eq. (9) is 0.863. The comparison of the experimental data with the values calculated by Eq. (9) is shown in Fig. 11(a). The properties in the dimensionless numbers are evaluated at the arithmetically mean value of the liquid temperature at the inlet and the melting temperature. The density of melt from ice particles is greater than that of ice particle and mainstream water (except for the case of $T_{l0} = 4$ °C), causing natural convection to occur. The non-floating packing pattern normally occurs when the value of Gr/Re^2 is low. In this study, it corresponds to $0.000151 \leqslant Gr/Re^2 \leqslant 0.00443$. Within this range, the influence of natural convection on the heat transfer can be neglected. Therefore, the Grashof number is not included in Eq. (9).

The mixed convection occurs in the floating packed bed. It corresponds to $0.00528 \leqslant Gr/Re^2 \leqslant 12.14$ in this study. The empirical correlation for the average heat transfer coefficient between the flow and melting particles in the floating packed bed is obtained as follows:

$$Nu = 2 + 2.50 \times 10^{-3} Re^{0.45} Gr^{0.355} Pr^{1/3} Ste^{-1.29}, \quad (10)$$

which is valid for

$46 \leqslant Re \leqslant 2291$, $0.00528 \leqslant Gr/Re^2 \leqslant 12.14$, and $0.228 \leqslant Ste \leqslant 0.385$.

An R^2 value for Eq. (10) is 0.961. The comparison of the experimental data with the values calculated by Eq. (10) is shown in Fig. 11(b).

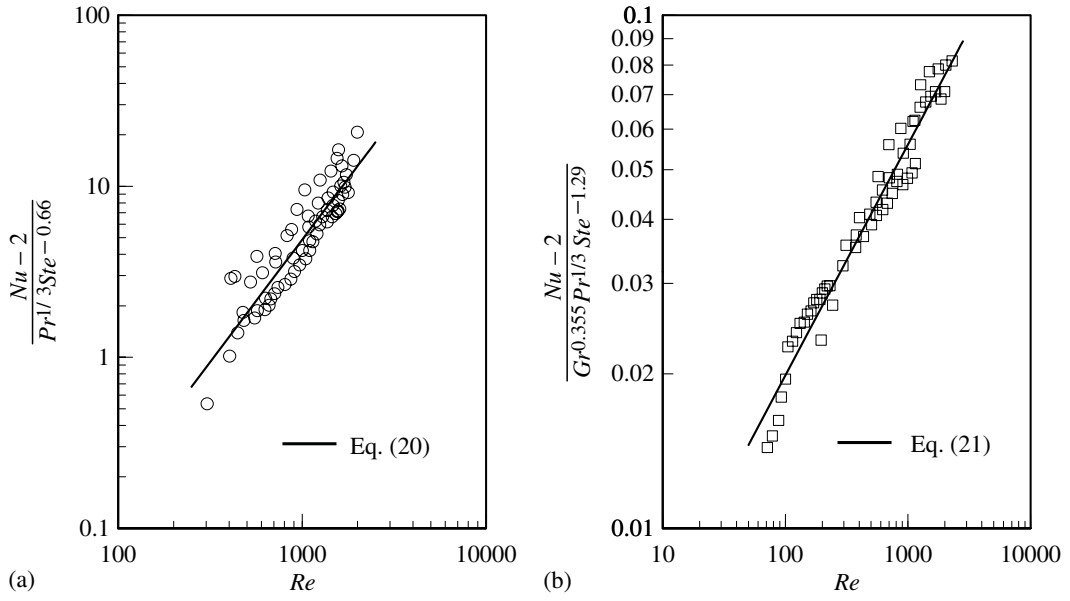

Fig. 11. Correlations for (a) non-floating packed bed and (b) floating packed bed.

3.5. Critical condition for the packing pattern change

As discussed above, there is a significant difference in heat transfer characteristics between the two types of packing pattern. Predicting which type of packing pattern occurs is important for the practical purpose. An effort has been attempted to characterize the critical condition of the change from the floating packed bed to the non-floating packed bed.

Five sequences of experiments are carried out under the conditions of the initial volume diameter of 26.2 mm, the initial ice temperature of −20 °C, and the initial mass of 0.5, 1.0, and 2.0 kg, respectively, and different water inlet velocities and temperatures. The observations from the 53 cases indicate that the transition from the floating packing to the non-floating packing pattern in a melting packed bed is a complex phenomenon. The drag force exerted on the particles by the fluid, buoyancy force of the surrounding fluid and initial pattern of the packed bed play the dominant roles in the process. The interactions between particles and the geometry of channel also play important roles. The effect of the interactions between particles during the melting process is very difficult to be quantified. As the first attempt, we propose using the ratio of Reynolds number based on the water velocity, Re, and Reynolds number at the theoretical terminal velocity of the particle, Re_t, as the criterion of the packing pattern. The theoretical terminal velocity is defined from the instantaneous force balance between the buoyancy and drag forces exerting on the particle, and is a function of particle diameter and temperature only.

Fig. 12 shows the ratio and corresponding packing pattern in the 53 cases. The results indicate that the range of ratio (Re/Re_t) in the present study is divided into three regions by two dashed lines, $Re/Re_t = 0.3175$ and $Re/Re_t = 0.4013$, respectively. The three regions are defined as the floating packing, transition, and non-floating packing regions, as shown in Fig. 12. When the ratio (Re/Re_t) is less than 0.3175, the floating packing pattern appears during the melting process. When the ratio (Re/Re_t) is greater than 0.4013, the non-floating packing pattern appears. When the value of (Re/Re_t) is between 0.3175 and 0.4013, either packing pattern may exist.

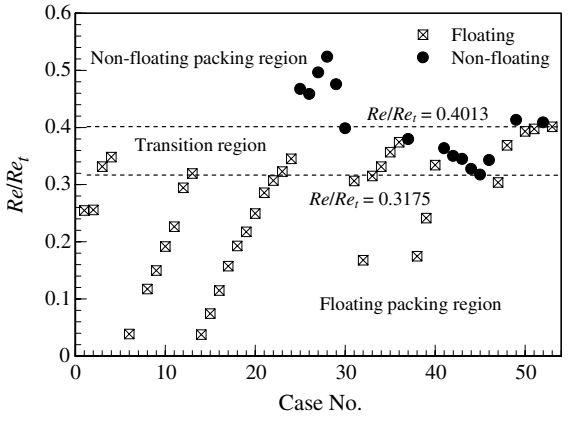

Fig. 12. Critical conditions for the change of packing pattern of melting packed beds.

4. Conclusions

The experiments for a melting packed beds subject to a horizontal flow of the same species at a non-equilibrium temperature have been conducted. The typical melting processes have been characterized by varying the mainstream velocity, supplied temperatures and initial mass of packed bed. The average melting rate per unit bed volume, average heat transfer coefficient and correlations for Nusselt number have been determined. Two types of packing pattern of melting packed bed under the different flow conditions have been identified as floating and non-floating packing patterns. Based on the experimental results, the following conclusions may be drawn:

(1) The surface area per unit bed volume increases as the time elapses during the melting process, resulting in the increase in the average melting rate per unit bed volume with time.
(2) The supplied velocity and temperature are the main controlling variables for a melting process. A higher supplied velocity or a higher temperature results in the higher average melting rate per unit bed volume.
(3) The packing pattern of ice particles also influences the melting process. The uniform and tight packing pattern leads to a high average melting rate per unit bed volume.
(4) There exists a significant difference in the heat transfer characteristics between the two types of packing pattern. The average heat transfer coefficient decreases with time during the melting process for a floating packed bed, while for a non-floating packed bed it remains nearly constant. In general, the average heat transfer coefficient for a non-floating packed bed is greater than that for a floating packed bed.
(5) The average heat transfer coefficient increases with the velocity. The effect of water temperature on the average heat transfer coefficient is not significant in the range studied. Two separate correlations of the Nusselt number are presented for the floating and non-floating packing patterns.
(6) Using the definition of the terminal velocity, the Reynolds number ratio, Re/Re_t can be used as a criterion defining the packing pattern. When Re/Re_t is

lower than 0.3175, the floating packing pattern prevails. Re/Re_t is greater than 0.4013 when the non-floating packing pattern exists. For Re/Re_t in between 0.3175 and 0.4013, a transitional packing pattern is defined.

(7) The density of water reaches its peak value at 4 °C. Because of this density inversion, different characteristics of packing pattern and heat transfer from those under other conditions are observed. The packed bed of ice particles in the mainstream water at 4 °C tends to have a higher volume fraction of ice particles, which approaches nearly a constant during melting. The average heat transfer coefficient in this case is slightly lower than those under the condition of higher supply temperature.

Acknowledgements

The supports from NASA (Grant No. NAG3-1797) and NSF (Grant No. HRD 6706268) are greatly appreciated. The assistances from Ryan Moreno and Julian Blanch on data collection and processing are also acknowledged.

References

[1] S. Fukusado, M. Yamada, Recent advance in research on water-freezing and ice-melting problems, Exp. Therm. Fluid Sci. 6 (1993) 90–105.

[2] D.A. Kearns, G.A. Plumb, Direct contact melting of a packed bed, ASME J. Heat Transfer 117 (2) (1995) 452–457.

[3] Y.-X. Tao, G. Vidhuvalavan, S. Sabau, Characterization of convective melting of granular porous, in: B.F. Armaly et al. (Eds.), ASME Proceedings of the 7th AIAA/ASME Joint Thermophysics and Heat Transfer Conference, Albuquerque, NM, HTD-Vol. 357-3, 1998, pp. 13–21.

[4] Y.L. Hao, Y.-X. Tao, Heat transfer characteristics of melting ice spheres under forced and mixed convection, J. Heat Transfer 124 (5) (2002) 891–903.

[5] G.A. Plumb, Convective melting of packed beds, Int. J. Heat Mass Transfer 37 (5) (1994) 829–836.

[6] J. Pak, O.A. Plumb, Melting in a two-component packed bed, J. Heat Transfer 119 (3) (1997) 553–559.

[7] A.S. Sabau, Y.-X. Tao, On mathematical modeling of convective melting of a granular porous medium, in: K. Goodson et al. (Eds.), ASME Proceedings of the 32nd National Heat Transfer Conference, Baltimore, MD, HTD-Vol. 349, 1997, pp. 197–204.

[8] J. Jiang, J. Sun, V. Ganesan, Y.-X. Tao, Numerical modeling of two-dimensional convective melting of granular packed beds, in: M.K. Jensen, M. Di Marzo (Eds.), ASME Proceedings of the 33rd National Heat Transfer Conference, Albuquerque, NM, NHTC99-216, 1999.

[9] Y.L. Hao, Y.-X. Tao, Non-thermal equilibrium melting of granular packed bed in horizontal forced convection. Part II: numerical simulation, Int. J. Heat Mass Transfer, in press.

[10] V. Alexiades, A.D. Solomon, Mathematical Modeling of Melting and Freezing Processes, Hemisphere Publishing Corporation, Washington, 1993, pp. 117–120.

[11] R.J. Moffat, Describing the uncertainties in experimental results, Exp. Therm. Fluid Sci. 1 (1988) 3–17.